ChemComm

Accepted Manuscript

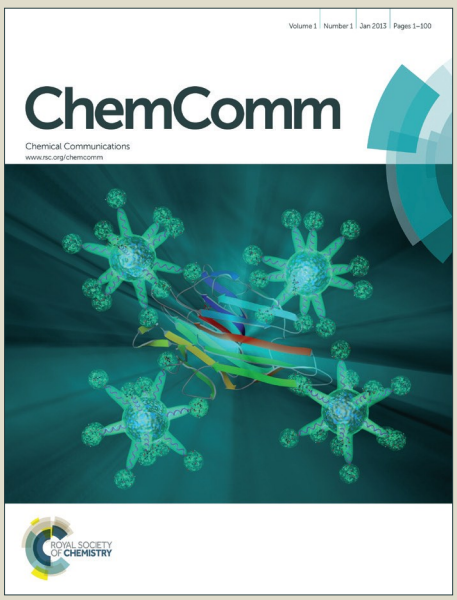

ROYAL SOCIETY OF CHEMISTRY

www.rsc.org/chemcomm

Journal Name

COMMUNICATION

Polystyrene sphere-mediated ultrathin graphene sheets-assembled frameworks for high-power density Li-O_2 batteries

Received 00th January 20xx,
Accepted 00th January 20xx

DOI: 10.1039/x0xx00000x

www.rsc.org/

Chang Yu,[#] Changtai Zhao,[#] Shaohong Liu, Xiaoming Fan, Juan Yang, Mengdi Zhang and Jieshan Qiu*

Free-standing, polystyrene sphere-mediated ultrathin graphene sheets-assembled aerogels (PGA) with open and interconnected porous framework were configured, indicative of the high energy density and high power density as a binder-free cathode for Li-O_2 batteries.

Rechargeable Li-O_2 batteries have received intense interest because of the ultrahigh theoretical specific energy.[1-3] With this in mind, Li-O_2 batteries become one of very potential candidates for fulfilling the practical application in the electric vehicles (EVs).[4, 5] Nevertheless, there is still a challenge on how to achieve a high energy density with a high power density which is necessary for EVs, due to the seriously sluggish oxygen reduction reaction (ORR) and oxygen evolution reaction (OER) in Li-O_2 batteries.[6, 7] The development of the efficient cathode materials of Li-O_2 batteries is one of effective strategies to meet these requirements.

It is not uncommonly believed that the cathode materials with open and interconnected channels as well as abundant macropores are beneficial to deposit discharge products and further lead to an increase of specific capacity.[8, 9] Such a structure can continuously and rapidly supply O_2 and Li^+ into the interior region of the air electrode, even when it is during deep discharge and fast discharge process.[10, 11] Meanwhile, 3D interpenetrating and conductive frameworks can achieve the rapid transportation of electron in the whole electrode networks.[12] The rapid transportation of O_2, Li^+ and electron can decrease the resistance and polarization of ORR and OER and further improve the rate performance and reduce the overpotential of batteries to a great degree. To date, various porous carbon electrodes[13-21] have been developed to achieve increased capacities. However, the rate capability is still far from satisfactory possibly due to the poorly designed electrode architectures. Therefore, the reasonable design of electrode materials with superior structure will become more potential to fulfil the practical application.

Graphene as a 2D star electrode material has been used in various energy storage and conversion devices due to its unique properties.[22-24] Moreover, it can be assembled into 3D monolith materials, of which 3D graphene aerogels have a wide range of pore free-standing structure, as well as high conductivity networks.[25] Such unique characteristics would be favorable for high-performance Li-O_2 batteries. However, of the 3D graphene aerogels available now, their assembling is directly achieved via hydrothermal method in the presence of graphene oxide (GO), leading to non-controllable intrinsic structure.[25] This will also affect and inhibit its electrochemical performance to a great degree. With this information, 3D aerogels composed of ultrathin, multi-wrinkled, and highly active 2D graphene sheets, and with open and interconnected channels are sought after for high-performance electrodes in Li-O_2 batteries.

Herein, we report a strategy for configuring polystyrene (PS) sphere-mediated ultrathin graphene sheets-assembled aerogels (PGA) via one-pot hydrothermal method followed by the high temperature annealing (as shown in Fig. S1), in which PS spheres have dual roles: template for interconnected pore formation, dispersant for protecting GO from aggregating or excessive π-π stacking and leading to the formation of ultrathin graphene due to the existing electrostatic repulsion between GO nanosheets and PS spheres. The as-obtained PGA as the binder-free air electrode in Li-O_2 batteries exhibits an ultrahigh specific capacity (21507 mA h g^{-1}), rate capabilities (4652 mA h g^{-1} at 2400 mA g^{-1}) and an electrocatalyst-like behavior with reduced overpotential.

The morphology of as-made samples was characterized using scanning electron microscopy (SEM) and transmission electron microscopy (TEM). From Fig. 1a, Fig. S2 and Fig. S3, it can be clearly seen that PS spheres can be uniformly wrapped in the graphene sheets. It is very interesting that compared with the as-obtained GO (Fig. S4) in the absence of PS spheres, a loose unordered structure and relatively multi-wrinkle and ultrathin graphene sheets can be clearly observed in the PGA (Fig. 1b,c) when PS spheres were removed by annealing. Further TEM image (Fig. 1d) reveals that the graphene sheets of PGA are relatively multi-wrinkle compared with

Carbon Research Laboratory, Liaoning Key Lab for Energy and Chemical Engineering, State Key Lab of Fine Chemicals, School of Chemical Engineering, Dalian University of Technology, Dalian, 116024, China. Tel: +86-411-84986080, Email: jqiu@dlut.edu.cn

† Electronic Supplementary Information (ESI) available: details of experimental method, characterization, electrochemical test, Fig.S1–S24. See DOI: 10.1039/c000000x/

 # The first two authors contributed equally to this work.

that of GA (Fig. S5). The reason for this would be that the PS spheres can act as the template to create lots of macropores and modulate the assembly of graphene during hydrothermal and annealing process. Meanwhile, PS spheres as scaffolds or supports can also effectively protect GO from aggregating during the hydrothermal process, leading to relatively multi-wrinkle and thin graphene sheets.

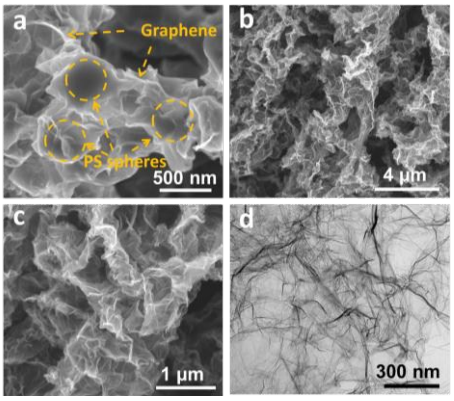

Fig. 1 SEM images of PEGA (a) and PGA (b, c); (d) TEM image of PGA.

Moreover, it is worth noting that the volume of the graphene aerogels has an increase when the PS spheres are present in comparison to that in the absence of PS spheres (Fig. S8a), further confirming the open pore structure formation within PGA matrix. These characteristics are also further confirmed through a high porosity of 99.81% on PGA and a low volume density of PGA (4.2 mg cm^{-3}), being a decrease of ca. 20% than that of GA (5.2 mg cm^{-3}, as shown in Fig. S9).

The relatively loose and open interconnected structure as well as ultrathin characteristics of graphene sheets within PGA matrix also can be further confirmed by the nitrogen physical adsorption results (Fig. S10). As shown in Fig. S10a, a combined characteristic of type I/IV isotherms can be observed, demonstrating a wide range of pore structure of the samples, which will be further confirmed by pore distribution results shown in Fig. S10b. It is also noted that the micropores in range of 0.5-1 nm and the large mesopores and macropores from 10-100 nm are present in both samples, which is also a common characteristics of graphene aerogels.[25] Compared with BET surface area (244 m^2 g^{-1}), mesopore and marcopore volumes (0.63 cm^3 g^{-1}) of GA, the as-made PGA sample shows an increasing BET surface area of 602 m^2 g^{-1} and large volumes of mesopore and marcopore (2.20 cm^3 g^{-1}), being nearly an increase of 249%. This further confirms the dual roles of PS spheres: template for interconnected pore formation, dispersant for protecting GO from aggregating or excessively stacking.

The electrochemical performance of the as-prepared PGA as cathode for Li-O_2 cells was tested with TEGDME electrolyte containing 1 M $LiPF_6$. Surprisingly, the PGA air electrode delivers an ultrahigh discharge capacity of 21507 mA h g^{-1} at a current density of 200 mA g^{-1} (corresponding to the volumetric energy density of 240 mWh cm^{-3}), which is higher than that of the GA electrode (9313 mA h g^{-1}) (Fig. 2a). Fig. 2b-c show the first discharge capacity of PGA and GA electrodes at increasing current densities of 400, 800, 2400, and 4000 mA g^{-1}. It is surprising that the discharge capacities of PGA electrodes can still reach to 13271 and 10000 mA h g^{-1}, respectively, even if at higher current densities of 400 and 800 mA g^{-1}. In this case, the GA air electrodes only exhibit low rate capacities of 57[illegible] and 4520 mA h g^{-1}. Even increasing the current densities to 2.4 A g^{-1} and 4 A g^{-1}, the discharge capacities of PGA electrodes still can reach to 4652 mA h g^{-1} and 1862 mA h g^{-1}, respectively. Compared with the recent reports on graphene based air electrode materials, the as-obtained PGA shows outstanding and unique specific capacity and rate capacity especially at high current densities (for detail, see Fig. S15). Based on the total mass of C+Li_2O_2, gravimetric energy density of PGA-O_2//Li cell reaches to 1400 Wh kg^{-1} at a power density of 3400 W kg^{-1}, indicating significant advantages of high energy density and high power density compared with Ni-MH batteries and Li-ion battery and matching the level of engine driven systems (shown in Fig. 2d).[26, 27] Such high specific capacity and rate capacity would be attributed to the superior pore structure and 3[illegible] conducting network of PGA, which will also confirmed by the following the electrochemical impedance spectra (EIS) results (Fig. S16).

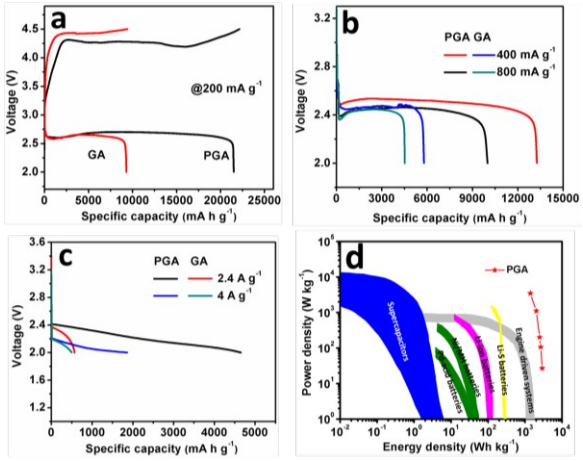

Fig. 2 (a) The discharge-charge curves of Li-O_2 cell using PGA and GA electrodes; (b, c) The rate capabilities of the Li-O_2 cells based on PGA and GA air electrodes; (d) Ragone plot of the Li-O_2 batteries with PGA as air electrode (based on the total mass of C+Li_2O_2).

It is interesting that compared with GA electrode, the PGA electrode decrease the overpotential, exhibiting an electrocatalyst-like behavior (Fig. 3a). When the cells were discharged and recharged to the capacity of 3000 mA h g^{-1}, the PGA electrode shows a lower charge overpotential and discharge overpotential than that of GA electrode. In order to further probe the catalytic action of PGA electrode, cyclic voltammetry (CV) measurement was performed, and the result is shown in the Fig. 3b. Compared with GA electrode, the PGA electrode presents a high ORR onset potential, a low OER onset potential, and relatively large ORR and OER peak currents, implying that catalytic activity is enhanced for both the ORR and OER, which is well consistent with the charge-discharge results. Further, the cycling performance (Fig. 3c) was investigated by fixing the capacity of 1000 mA h g^{-1}, indicative of a relatively ordinary cycle life of 42 cycles. The reason for this is attributed to the generation of a large amount of side products and the inferior decomposition ability of discharge products during charge process. It can be confirmed by the changes of the electrode morphology (Fig. S20) and changed impedance (Fig. 3d) at the different cycling states. Moreover, the discharge products of the PGA electrode were also examined by the X-ray diffraction (Fig. S21) and Fourier transform infrared spectrometer (FTIR) techniques (Fig.

S22), demonstrating that the discharge products are mainly composed of Li_2O_2 and the side products such as LiOH, $LiCO_3$, HCO_2Li and CH_3CO_2Li etc. These side products and undecomposed discharge product Li_2O_2 are responsible for relatively ordinary cycle life.

The structure of the PGA electrode after the partial discharge (fixed capacity of 2000 mA h g^{-1}) and full discharge was examined by SEM, and the results are shown in Fig. S23. It can be clearly seen that the discharge products uniformly deposits on the surface of graphene sheets at the beginning of discharge (Fig. S23a). After the full discharge, all the void space of the electrode next to the separator is filled with discharge products and no more pores are available for O_2 transportation (Fig. S23b). This indicates O_2 and Li^+ can smoothly pass through the entire electrode to the reaction sites near the separator even if in the case of deep discharge. Moreover, such a high density deposition of discharge products demonstrates the thoroughness of the electrochemical reactions in PGA electrode and further verifies the highly efficient utilization of the interconnected porous structure.

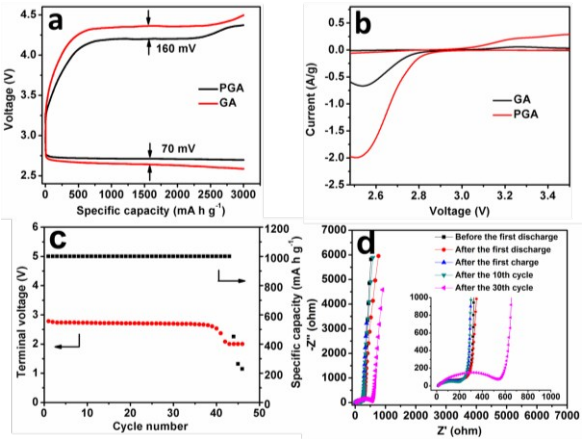

Fig. 3 (a) The discharge-charge curves of Li-O_2 cells using PGA and GA electrodes with a fixed capacity of 3000 mA h g^{-1}; (b) CV curves of the PGA and GA electrodes at a scanning rate of 0.1 mV s^{-1}; (c) The cycling performance of PGA electrode; (d) Nyquist plots of PGA electrode at different discharge states.

The above results demonstrate that the PGA as binder-free Li-O_2 cell electrode shows an electrocatalyst-like behavior with decreasing overpotential, and superior specific capacity and rate capability can be delivered. Such an excellent performance can be attributed to the unique architectural features. The abundant unordered macropores within the PGA provide enough void volume for accommodating the discharge products, thus resulting in a much enhanced discharge capacity. And interconnected porous channels can store lots of electrolyte and facilitate continuous and rapid transportation of O_2 and Li^+ during deep and fast discharge process. The interpenetrating graphene networks can ensure rapid supply of electrons. The as-formed 2D ultrathin graphene nanosheets within aerogel wall can shorten ion transport distance in nano-scaled dimension to some extent. These combined characteristics make low reaction resistances of ORR/OER, promoting the rates of ORR/OER, thus leading to excellent rate capability and the reduced overpotentials.

In summary, graphene aerogels made of ultrathin and multi-wrinkle graphene nanosheets have been successfully prepared by PS spheres colloidal template-assisted method. The as-obtained PGA assembled via ultrathin and multi-wrinkle graphene sheets demonstrates open and interconnected porous netwo characteristics. As a free-standing air electrode for Li-O_2 batterie an ultrahigh specific capacity and rate capability and reduce overpotentials can be delivered. This demonstrates PGA promising cathode material of Li-O_2 batteries with high energ density and power density.

This work was partly supported by the NSFC (Nos. U1203292 ar 21336001), the Education Department of Liaoning Province of China (T2013001), and the Fundamental Research Funds for the Centr Universities (DUT14LAB06).

Notes and references

1. P. G. Bruce, S. A. Freunberger, L. J. Hardwick and J.-M. Tarascon, *Na Mater.*, 2012, **11**, 19-29.
2. G. Girishkumar, B. McCloskey, A. C. Luntz, S. Swanson and W. Wilcke *J. Phys. Chem. Lett.*, 2010, **1**, 2193-2203.
3. J.-S. Lee, S. Tai Kim, R. Cao, N.-S. Choi, M. Liu, K. T. Lee and J. Cho, *Energy Mater.*, 2011, **1**, 34-50.
4. B. Sun, P. Munroe and G. Wang, *Sci. Rep.*, 2013, **3**.
5. S. Liu, Y. Zhu, J. Xie, Y. Huo, H. Y. Yang, T. Zhu, G. Cao, X. Zhao and S. Zhang, *Adv. Energy Mater.*, 2014, **4**, n/a-n/a.
6. S. Liu, Z. Wang, C. Yu, Z. Zhao, X. Fan, Z. Ling and J. Qiu, *J. Mater. Chem. A*, 2013, **1**, 12033-12037.
7. F. Li, T. Zhang and H. Zhou, *Energy Environ. Sci.*, 2013, **6**, 1125-1141.
8. Q. Li, R. Cao, J. Cho and G. Wu, *Phys. Chem. Chem. Phys.*, 2014, **16**, 13568-13582.
9. X. Lin, L. Zhou, T. Huang and A. Yu, *J. Mater. Chem. A*, 2013, **1**, 123 1245.
10. B. Sun, X. Huang, S. Chen, P. Munroe and G. Wang, *Nano Lett.*, 2014, **14**, 3145-3152.
11. H.-D. Lim, K.-Y. Park, H. Song, E. Y. Jang, H. Gwon, J. Kim, Y. H. Kim, M D. Lima, R. O. Robles, X. Lepró, R. H. Baughman and K. Kang, *Adv. Mater.*, 2013, **25**, 1348-1352.
12. Y. Zhao, J. Liu, Y. Hu, H. Cheng, C. Hu, C. Jiang, L. Jiang, A. Cao and L. Qu, *Adv. Mater.*, 2013, **25**, 591-595.
13. W.-H. Ryu, T.-H. Yoon, S. H. Song, S. Jeon, Y.-J. Park and I.-D. Kim, *Nano letters*, 2013, **13**, 4190-4197.
14. Y. Chen, F. Li, D.-M. Tang, Z. Jian, C. Liu, D. Golberg, A. Yamada and H. Zhou, *J. Mater. Chem. A*, 2013, **1**, 13076-13081.
15. R. R. Mitchell, B. M. Gallant, C. V. Thompson and Y. Shao-Horn, *Energy Environ. Sci.*, 2011, **4**, 2952-2958.
16. J. Park, Y.-S. Jun, W.-r. Lee, J. A. Gerbec, K. A. See and G. D. Stucky, *Chem. Mater.*, 2013, **25**, 3779-3781.
17. Z. Zhang, L. Su, M. Yang, M. Hu, J. Bao, J. Wei and Z. Zhou, *Chem. Commun.*, 2014, **50**, 776-778.
18. Z. Guo, D. Zhou, X. Dong, Z. Qiu, Y. Wang and Y. Xia, *Adv. Mater.*, 2013, **25**, 5668-5672.
19. Z. Zhang, J. Bao, C. He, Y. Chen, J. Wei and Z. Zhou, *Adv. Funct. Mate* 2014, **24**, 6826-6833.
20. Z.-L. Wang, D. Xu, J.-J. Xu, L.-L. Zhang and X.-B. Zhang, *Adv. Funct. Mater.*, 2012, **22**, 3699-3705.
21. G. Wu, N. H. Mack, W. Gao, S. Ma, R. Zhong, J. Han, J. K. Baldwin and P. Zelenay, *ACS Nano*, 2012, **6**, 9764-9776.
22. W. Zhang, J. Zhu, H. Ang, Y. Zeng, N. Xiao, Y. Gao, W. Liu, H. H. Hng and Q. Yan, *Nanoscale*, 2013, **5**, 9651-9658.
23. Y. Cao, Z. Wei, J. He, J. Zang, Q. Zhang, M. Zheng and Q. Dong, *Energy Environ. Sci.*, 2012, **5**, 9765-9768.
24. Y. Li, J. Wang, X. Li, D. Geng, R. Li and X. Sun, *Chem. Commun.*, 2011, **47**, 9438-9440.
25. Y. Li, J. Chen, L. Huang, C. Li, J.-D. Hong and G. Shi, *Adv. Mater.*, 2014, **26**, 4789-4793.
26. P. Simon and Y. Gogotsi, *Nat. Mater.*, 2008, **7**, 845-854.
27. H.-J.Peng, J.-Q. Huang, M.-Q. Zhao, Q. Zhang, X.-B. Cheng, X.-Y. Liu, W.-Z. Qian, and F. Wei, *Adv. Funct. Mater.*, 2014, **24**, 2772-2781.